Acta Universitatis Sapientiae
Electrical and Mechanical Engineering, 11 (2019) 54-66

DOI: 10.2478/auseme-2019-0005

An Eight-Node Hexahedral Finite Element with Rotational DOFs for Elastoplastic Applications

Ayoub AYADI[1], Kamel MEFTAH[1], Lakhdar SEDIRA[2], Hossam DJAHARA[1]

[1] Laboratoire de Génie Energétique et Matériaux (LGEM), University of Biskra, BP145 RP Biskra, Algeria, e-mail: a.ayadi@univ-biskra.dz, k.meftah@univ-biskra.dz, hossam.djahara@ univ-biskra.dz
[2] Laboratoire de Génie Mécanique (LGM), University of Biskra, BP145 RP Biskra, Algeria, e-mail: l.sedira@univ-biskra.dz

Manuscript received January 21, 2019; revised May 14, 2019.

Abstract: In this paper, the earlier formulation of the eight-node hexahedral SFR8 element is extended in order to analyze material nonlinearities. This element stems from the so-called Space Fiber Rotation (SFR) concept which considers virtual rotations of a nodal fiber within the element that enhances the displacement vector approximation. The resulting mathematical model of the proposed SFR8 element and the classical associative plasticity model are implemented into a Fortran calculation code to account for small strain elastoplastic problems. The performance of this element is assessed by means of a set of nonlinear benchmark problems in which the development of the plastic zone has been investigated. The accuracy of the obtained results is principally evaluated with some reference solutions.

Keywords: 3D finite elements, hexahedral elements, Space Fiber Rotation, elastoplasticity.

1. Introduction

Modeling physical phenomena leads in many cases to nonlinear problems. In structural engineering, elastoplastic analysis is important for a wide range of industrial processes and many applications might be a source of material nonlinearities. For instance, in automobile and aerospace industries, crash-worthiness is a major area of interest. Another example is metal forming processes, where tests in the design of new products are required to evaluate their performance. More recently, drop impact test of some mobile devices such as mobile phones, personal digital assistants and laptops which involve plastic deformation have been an object of research [1]. As these tests are high priced,

nonlinear finite element analysis has emerged as a viable alternative in addressing these kinds of problems. As a matter of fact, the finite element method is considered the most adopted procedure for solving elastoplastic problems [2]. Since the first published papers addressing elastoplastic problems using finite element method in the mid-1960s [3-6], the debate about accuracy and efficiency of finite elements in nonlinear structural analysis has gained fresh prominence. As a result, many shell, solid, as well as solid-shell element formulations have been developed and extended to nonlinear problems involving elastoplastic analysis. Surveys such as that conducted by Yang et al. [7] compiles the important literature on shell finite elements in both linear and nonlinear regimes. It includes several techniques to improve classical shell element efficiency as they suffer from some undesirable responses such as locking phenomenon and zero energy modes. However, the classical shell element formulations carry with them various limitations especially when information across the thickness is required as in hydroforming process and draw-bending tests [8].

To solve this problem, several shell formulations have been proposed to take the thickness stretch into consideration (see [9-11] to cite only a few). Despite these pioneering achievements, solid-shell elements have emerged as a powerful platform for modeling elastoplastic problems [12-15] as they provide many advantages with respect to shell elements such as the natural treatment of double-sided contact and the straightforward connection with solid elements. On the other hand, many solid elements have been also developed to address a large set of linear and nonlinear problems [16-18] as they offer easier formulation, in comparison with shell elements, based on three dimensional constitutive laws. May et al. [19], investigated the elastoplastic behavior of beams under pure and warping torsion using a 20-noded isoparametric brick element. In order to overcome some well-known deficiencies of the classical first-order element, including volumetric locking, Roehl and Ramm [20] developed two enhanced elements denoted by HEXA8-E3 and HEXA8-E6 based on the enhanced assumed strain concept to account for large elastoplastic analysis of solids and shells. In the same context, Liu et al. [21] suggested four-point quadrature hexahedral element in which the shear locking was avoided by means of generalized strain vector written in a local corotational system. To improve the elastoplastic analysis of irregular meshes, Cao et al. [22] proposed a brick element where a penalty term is introduced into the Hu-Washizu functional to enforce stresses to satisfy the equilibrium equations. Also, Wang and Wagoner [8] developed the so-called WW3D solid element, a mixed eight-node hexahedral element, for sheet forming analysis where the strain components corresponding to locking modes are eliminated. Recently, Artioli et al. [23] proposed a linear hexahedral element based on the assumed strain

technique. This element has its origins in the Nodally Integrated Continuum Element (NICE) formulation [24] and it was successfully implemented to solve plasticity problems.

This study aims at investigating a recently published 3D solid element performance, named SFR8, in small strain nonlinear elastoplastic problems. The element's formulation is based on the so-called Space Fiber Rotation (SFR) approach firstly proposed by Ayad [25]. This approach considers 3D rotations of a virtual fiber within the finite element that improves the displacement vector approximation. Hence, the SFR concept adds rotational DOFs along with the classical displacement ones. Ayad et al. [26] adopted the SFR concept to formulate two eight-node hexahedral elements SFR8 and SFR8I. The response of these two elements in the linear static regime was examined through a series of benchmarks where the findings show a better accuracy than the classical first order hexahedral element and close to the quadratic 20-node hexahedral element. In the same vein, the SFR concept was adopted in the works of Meftah et al. [27, 28] to develop a six-node wedge element SFR6 and a multilayered hexahedral element SFR8M. In recent developments on the SFR elements, the SFR8 and the SFR8I elements were implemented into the commercial code ABAQUS by means of the UEL interface to address nonlinear geometric problems [29]. The accuracy of the proposed elements and especially the nonconforming element SFR8I was shown to be close to that of the ABAQUS quadratic element C3D20.

The remaining part of the paper proceeds as follows. In the following section, the general formulation of the eight-node hexahedral element SFR8 is presented. Then, the constitutive model for small strain elastoplasticity is described briefly. The third section is concerned with the nonlinear finite element procedure. Finally, and before highlighting the concluding remarks, the performance of the proposed SFR8 element is assessed through a variety of nonlinear elastoplastic problems.

2. Kinematics of the SFR concept

This section details the formulation of the SFR8 hexahedral finite element. As shown in *Fig. 1*, this formulation is based on the so-called Space Fiber concept which considers a virtual nodal fiber within the element (fiber $\overline{iq}$). This fiber rotation, defined by the rotation vector $\overline{\theta_i}$, develops additional displacements that enhance the classical approximation of the displacement vector. Accordingly, the final displacement field takes the following form:

$$\overline{U}_q = \sum_{i=1}^{8} \left[N_i \overline{d_i} + f\left(\overline{\theta_i}, \overline{iq}\right) \right] \tag{1}$$

where $f(\overline{\theta_i}, \overline{iq})$ is the additional displacement vector, $\overline{d_i} = \{U_i V_i W_i\}^T$ is the vector of nodal displacements, and N_i are the classical shape functions associated with the eight-node brick element given by:

$$N_i(\xi,\eta,\zeta) = \frac{1}{8}(1+\xi_i\xi)(1+\eta_i\eta)(1+\zeta_i\zeta) \quad \text{with} \quad -1<\xi,\eta,\zeta<+1 \tag{2}$$

The additional displacement vector $f(\overline{\theta_i}, \overline{iq})$ is written as:

$$f(\overline{\theta_i}, \overline{iq}) = N_i(\overline{\theta_i} \wedge \overline{iq}) \tag{3}$$

where

$$\{iq\} = \{X_q - X_i\} = \begin{Bmatrix} X - X_i \\ Y - Y_i \\ Z - Z_i \end{Bmatrix} \quad ; \qquad \{\theta_i\} = \begin{Bmatrix} \theta_{Xi} \\ \theta_{Yi} \\ \theta_Z \end{Bmatrix} \tag{4}$$

X, Y, and Z are the global coordinates of q given by the following expressions

$$X = \sum_{i=1}^{8} N_i X_i \, ; \qquad Y = \sum_{i=1}^{8} N_i Y_i \, ; \qquad Z = \sum_{i=1}^{8} N_i Z_i \, , \tag{5}$$

where X_i, Y_i, Z_i are the global coordinates of node i.

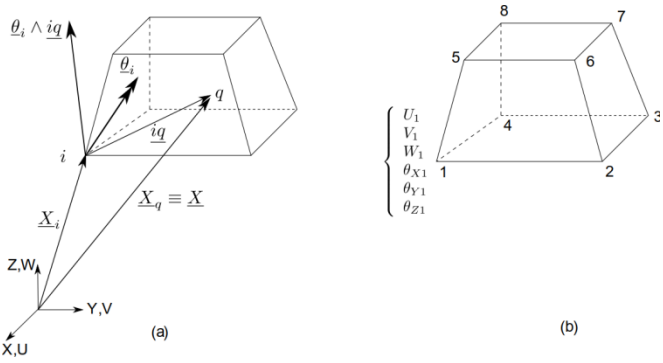

Figure 1: The SFR approach; (a) 3D rotation of the virtual fiber $\underline{iq}$ inducing an additional displacement, (b) the eight-node hexahedral element SFR8 and its nodal variables.

By performing the cross product $\overline{\theta_i} \wedge \overline{iq}$, we obtain the following approximation of the displacement vector (the Einstein summation convention on i is used):

$$\{U\} = \begin{Bmatrix} U \\ V \\ W \end{Bmatrix} = \begin{Bmatrix} N_i U_i + N_i (Z - Z_i)\theta_{Yi} - N_i (Y - Y_i)\theta_{Zi} \\ N_i V_i + N_i (X - X_i)\theta_{Zi} - N_i (Z - Z_i)\theta_{Xi} \\ N_i Y_i + N_i (Y - Y_i)\theta_{Zi} - N_i (X - X_i)\theta_{Xi} \end{Bmatrix}. \tag{6}$$

The approximation (6) can be expressed in a matrix form:

$$\{U\} = [N]\{d_n\} \quad ; \quad [N] = \begin{bmatrix} \{N_{ui}\}^T \\ \cdots \{N_{vi}\}^T \cdots i = 1,8 \\ \{N_{wi}\}^T \end{bmatrix} = \begin{bmatrix} \{N_u\}^T \\ \{N_v\}^T \\ \{N_w\}^T \end{bmatrix}, \tag{7}$$

where

$$\begin{aligned} \{N_{ui}\} &= \{N_i \quad 0 \quad 0 \quad 0 \quad N_i(Z - Z_i) \quad -N_i(Y - Y_i)\}^T \\ \{N_{vi}\} &= \{N_i \quad 0 \quad 0 \quad -N_i(Z - Z_i) \quad 0 \quad N_i(X - X_i)\}^T \\ \{N_{wi}\} &= \{N_i \quad 0 \quad 0 \quad 0 \quad N_i(Y - Y_i) \quad -N_i(X - X_i)\}^T \end{aligned} \tag{8}$$

and $$\{d_n\} = \{\cdots | U_i \quad V_i \quad W_i \quad \cdots \quad \theta_{Xi} \quad \theta_{Yi} \quad \theta_{Zi} | \cdots i = 1,8\}^T \tag{9}$$

is the global displacement vector of the SFR8 element.

3. Constitutive equation for rate independent elastoplasticity

After initial yielding, the total strain is made up additively of an elastic component ε^e and a plastic component ε^p so that:

$$\varepsilon_{ij} = (\varepsilon_{ij})^e + (\varepsilon_{ij})^p. \tag{10}$$

The elastic part of strain field is linked to stress field though the relation:

$$\sigma_{ij} = D^e_{ijkl}(\varepsilon_{kl} - \varepsilon^e_{kl}), \tag{11}$$

where D^e_{ijkl} is the tensor of elastic constants which for an isotropic material may be formulated as:

$$D^e_{ijkl} = G\left(\frac{2\nu}{1-2\nu}\delta_{ij}\delta_{kl} + \delta_{ik}\delta_{jl} + \delta_{il}\delta_{jk}\right), \tag{12}$$

in which G is the shear modulus; ν is Poisson's ration and δ_{ij} represents the Kronecker delta.

In this paper, the elastoplastic constitutive model based on the von Mises associated yield criterion is adopted. Therefore, the following yield function is considered.

$$f = \sigma_e - \sigma_y(\varepsilon^p) \leq 0, \tag{13}$$

where σ_e is the von Mises effective stress and σ_y is the yield stress which can be described by a nonlinear function of the equivalent plastic strain ε^p.

The plastic part of strain ε_{ij}^p is only defined by its increment $d\varepsilon_{ij}^p$ which, by using the normality flow rule, is given by:

$$d\varepsilon_{ij}^p = \bar{\lambda}\frac{\partial f}{\partial \sigma_{ij}} = \bar{\lambda}P, \tag{14}$$

where $\bar{\lambda}$ is a scalar function called the plastic multiplier, which determines the magnitude of plastic flow and P represents the direction of plastic strain rate.

Differentiation of (11) with respect to virtual time and combination of the result with Eq.14 and using the consistency condition $df = 0$, the plastic multiplier $\bar{\lambda}$ can be elaborated as:

$$\bar{\lambda} = \frac{(\partial f/\partial \sigma_{ij})D_{ijkl}^e d\varepsilon_{ij}}{(\partial f/\partial \sigma_{rs})D_{rstu}^e(\partial f/\partial \sigma_{tu}) + H_y}, \tag{15}$$

where H_y is the hardening moduli involved in the evolution laws describing the isotropic hardening.

By substituting the expression of the plastic multiplier $\bar{\lambda}$ into Eq. 11, the elastoplastic tangent modulus is derived as:

$$D_{ijkl}^{ep} = D_{ijkl}^e - \gamma\frac{D_{ijmn}^e(\partial f/\partial \sigma_{mn})(\partial f/\partial \sigma_{pq})D_{pqkl}^e}{(\partial f/\partial \sigma_{rs})D_{rstu}^e(\partial f/\partial \sigma_{tu}) + H_y}, \tag{16}$$

where $\gamma = 0$ for elastic loading/unloading, and $\gamma = 1$ for strict loading.

Finally, the complete elastoplastic stress strain relation can be expressed:

$$\sigma_{ij} = D_{ijkl}^{ep}\,\varepsilon_{kl}. \tag{17}$$

4. Numerical implementation

In order to solve the above nonlinear system, a two-step algorithm based on the state update procedure is adopted [30, 31]. The steps of the algorithm are:

1. Perform a predictor step in which we assume that the step (t_n, t_{n+1}) is elastic. Accordingly:

$$\varepsilon_{n+1}^{trail} = \varepsilon_n^e + \Delta\varepsilon \tag{18}$$

The corresponding trial stress is given by:

$$\sigma_{n+1}^{trail} = D\left(\varepsilon_{n+1} - \varepsilon_n^p\right) \tag{19}$$

2. Evaluation of the yield function
   If $f\left(\sigma_{n+1}^{trial}, H_y\right) \leq 0$, the stress lies within the yield surface and the trial state represents the actual final state of the material. Accordingly:

$$(\bullet)_{n+1} = (\bullet)_{n+1}^{trial} \tag{20}$$

   If $f\left(\sigma_{n+1}^{trial}, H_y\right) \geq 0$, the elastic trial state is not plastically admissible and the consistency condition is violated. Therefore, a plastic corrector step (or return mapping algorithm) is required.

An outline of the numerical procedure is provided in *Fig. 2*.

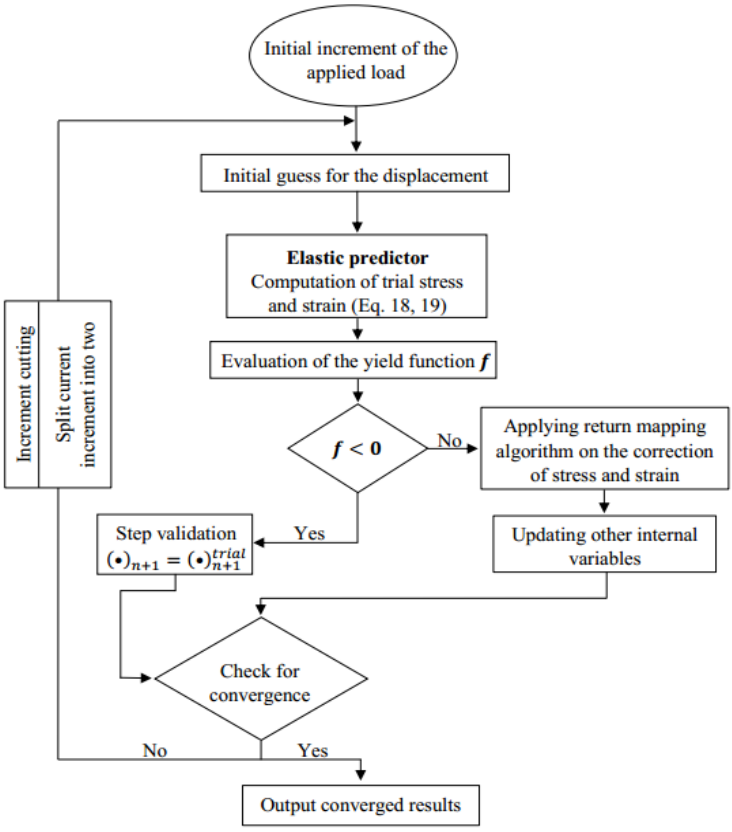

Figure 2: Flowchart of the numerical procedure.

5. Numerical examples

The proposed SFR8 element is implemented into HYPLAS software, a FORTRAN Finite Element code developed by de Souza Neto et al. [2] to account for hyperelastic and elastoplastic analysis. The performance of the SFR8 element, for elastoplastic problems, is evaluated with known benchmarks. The obtained results are compared with the ABAQUS Hybrid element C3D8H, the second-order ABAQUS hexahedral element C3D20, the NICE-H8 element developed by Artioli [23] and the standard hexahedral element H8.

5.1 Stretched perforated rectangular plate

In this example, a rectangular perforated plate subjected to longitudinal stretching is considered. This problem is frequently used as a benchmark to assess the precision and the effectiveness of the plasticity model as well as the adopted numerical technique. Material properties, geometric dimensions, boundary conditions and the finite element mesh of this example are all summarized in *Fig. 3*.

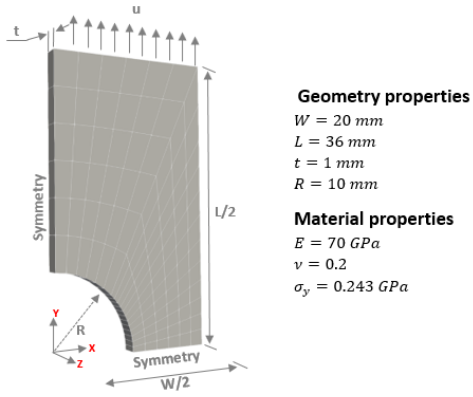

Figure 3: Stretched perforated plate: Geometry, FEM mesh and material properties.

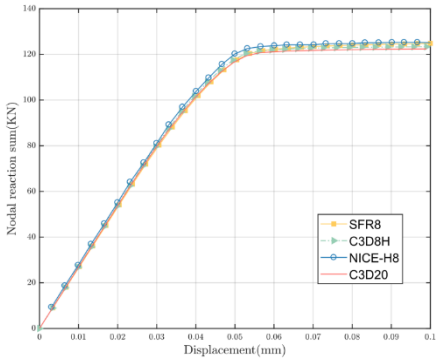

Figure 4: Stretched perforated plate: Reaction-displacement diagram.

A total displacement of 10 mm is applied on the upper edge of the plate. The final load is reached by performing 30 equal steps where the material is considered elastic perfectly plastic and the von Mises model is adopted. *Fig.4* shows the load deflection curve where the total reaction force at the bottom surface of the plate is plotted against the applied displacement. The results obtained by the SFR8 element are compared with some reference elements from the literature. The good agreement between the SFR8 element and the reference solutions is noticeable.

The evolution of the plastic strain is illustrated in *Fig.5.* Note that the first yielding is observed at the intersection of the Y-Symmetry plan and the edge of the hole where the plastic region extends in an oblique front along the entire cross section of the stretched plate.

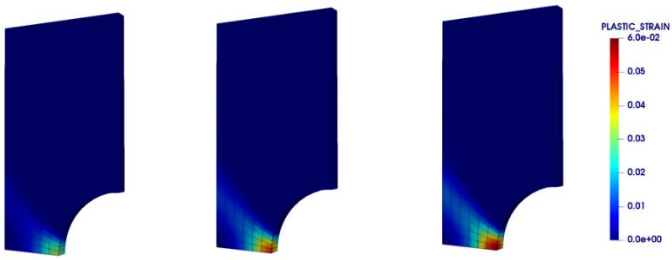

$\boldsymbol{u = 0.07\ mm}$ $\boldsymbol{u = 0.09\ mm}$ $\boldsymbol{u = 0.1\ mm}$

Figure 5: Stretched perforated plate: Equivalent plastic strain at different stages of the prescribed displacement.

5.2 Thick walled cylinder subjected to internal pressure

The second numerical example is illustrated in *Fig. 6*. This problem consists of an infinitely long, thick cylinder subjected to a gradually increasing internal pressure. This benchmark test has been studied by several authors [23, 32].

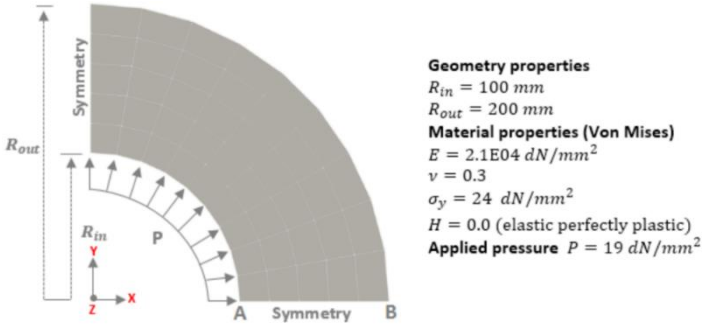

Figure 6: Thick cylinder: Geometry, Material properties and FE mesh.

Considering an elastic perfectly plastic material, the cylinder is assumed to have the properties shown in *Fig. 6.* Like the first example, only one quarter of the cylinder is considered where the boundary condition is assumed according to a plane strain condition assumed along the axis of the thick cylinder. The load is applied according to an incremental scheme of 10 equal steps.

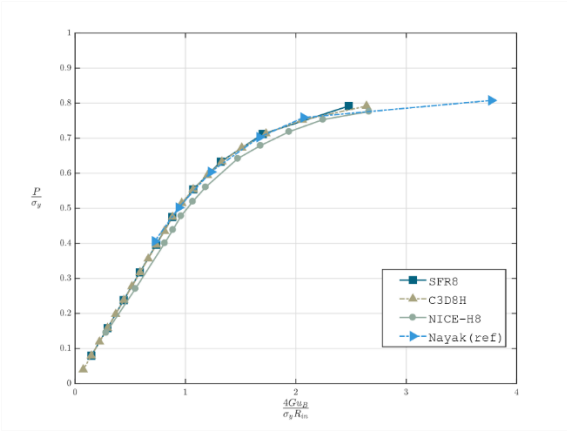

Figure 7: Thick walled cylinder: Pressure-displacement curve.

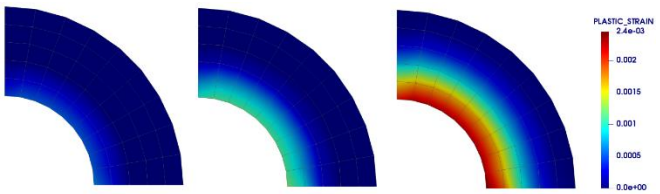

Figure 8: Thick walled cylinder: Evolution of the plastic deformation.

The pressure-displacement curve at point B is depicted in *Fig. 7* (G represents the shear modulus). The results obtained by the SFR8 element are compared with those given by ABAQUS as well as with the analytical solution taken from Nayak et al. [32]. It can be seen that the SFR8 element shows a good agreement with C3D8H, NICE-H8 element and the reference solution [32]. The evolution of the equivalent plastic strain is also illustrated in *Fig.7*. The plastic deformation starts at the inner surface and extends along the radius where it reaches a maximum of $\varepsilon_{Pmax}^{SFR8} = 0.0024$. When compared to ABAQUS results ($\varepsilon_{Pmax}^{C3D8H} = 0.002429$), the results are almost the same.

6. Conclusion

This work was designed to evaluate the performance of the SFR8 hexahedral element for small strain elastoplasticity analysis. The element formulation relies on the consideration of virtual rotations of a nodal fiber within the element that improves the displacement vector approximation. The adopted constitutive model is the classical associative von Mises plasticity model where the Newton-Raphson scheme has been implemented for solving the nonlinear numerical system. The element shows reliability and robustness when compared with some reference elements from the literature.

References

[1] Che, F. X., and Pang, J. H. “Study on Board-Level Drop Impact Reliability of Sn–Ag–Cu Solder Joint by Considering Strain Rate Dependent Properties of Solder”, *IEEE Transactions on Device and Materials Reliability*, vol. 15, no. 2, pp. 181-190, 2015.

[2] de Souza Neto, E. A., Peric, D., & Owen, D. R., “Computational methods for plasticity: theory and applications”, John Wiley & Sons, 2011.

[3] Pope, G. G., “A discrete element method for the analysis of plane elasto-plastic stress problems”, *The Aeronautical Quarterly*, vol. 17, no. 1, pp. 83-104, 1966.

[4] Marcal, P. V., & King, I. P., “Elastic-plastic analysis of two-dimensional stress systems by the finite element method”, *International Journal of Mechanical Sciences*, vol. 9, no. 3, pp. 143-155, 1967.

[5] Yamada, Y., Yoshimura, N., & Sakurai, T., "Plastic stress-strain matrix and its application for the solution of elastic-plastic problems by the finite element method", *International Journal of Mechanical Sciences*, vol. 10, no. 5, pp. 343-354, 1968.

[6] Oden, J. T., "Finite element applications in nonlinear structural analysis", in *Proceedings of the ASCE Symposium on Application of Finite Element Methods in Civil Engineering*, Vanderbilt University, 1969, pp. 419-456.

[7] Yang, H. T., Saigal, S., Masud, A., & Kapania, R. K., "A survey of recent shell finite elements", *International Journal for numerical methods in engineering*, vol. 47, no. 1-3, pp. 101-127, 2000.

[8] Wang, J., & Wagoner, R. H., "A practical large-strain solid finite element for sheet forming", *International journal for numerical methods in engineering*, vol. 63, no. 4, pp. 473-501, 2005.

[9] Brank, B., Korelc, J., & Ibrahimbegović, A., "Nonlinear shell problem formulation accounting for through-the-thickness stretching and its finite element implementation", *Computers & structures*, vol. 80, no. 9-10, pp. 699-717, 2002.

[10] Cardoso, R. P., & Yoon, J. W., "One point quadrature shell element with through-thickness stretch" *Computer Methods in Applied Mechanics and Engineering*, vol. 194, no. 9-11, pp. 1161-1199, 2005.

[11] Klinkel, S., Gruttmann, F., & Wagner, W., "A mixed shell formulation accounting for thickness strains and finite strain 3D material models", *International journal for numerical methods in engineering*, vol. 74, no. 6, pp. 945-970, 2008.

[12] Legay, A., & Combescure, A., "Elastoplastic stability analysis of shells using the physically stabilized finite element SHB8PS", *International Journal for Numerical Methods in Engineering*, vol. 57, no. 9, pp. 1299-1322, 2003.

[13] Abed-Meraim, F., and Combescure, A., "An improved assumed strain solid–shell element formulation with physical stabilization for geometric non-linear applications and elastic–plastic stability analysis", *International Journal for Numerical Methods in Engineering*, vol. 80, no. 13, pp. 1640-1686, 2009.

[14] Schwarze, M., Vladimirov, I. N., & Reese, S., "Sheet metal forming and springback simulation by means of a new reduced integration solid-shell finite element technology", *Computer Methods in Applied Mechanics and Engineering*, vol. 200, no. 5-8, pp. 454-476, 2011.

[15] Wang, P., Chalal, H., & Abed-Meraim, F., "Quadratic solid–shell elements for nonlinear structural analysis and sheet metal forming simulation", *Computational Mechanics*, vol. 59, no. 1, pp. 161-186, 2017.

[16] Mackerle, J., "Finite element linear and nonlinear, static and dynamic analysis of structural elements: a bibliography (1992-1995)", *Engineering Computations*, vol. 14, no. 4, pp. 347-440, 1997.

[17] Mackerle, J., "Finite element linear and nonlinear, static and dynamic analysis of structural elements–an addendum–A bibliography (1996-1999)", *Engineering computations*, vol. 17, no. 3, pp. 274-351, 2000.

[18] Mackerle, J., "Finite element linear and nonlinear, static and dynamic analysis of structural elements, an addendum: A bibliography (1999–2002)", *Engineering Computations*, vol. 19, no. 5, pp. 520-594, 2002.

[19] May, I. M., & Al-Shaarbaf, I. A. S., "Elasto-plastic analysis of torsion using a three-dimensional finite element model", *Computers & structures*, vol. 33, no. 3, pp. 667-678, 1989.

[20] Roehl, D., & Ramm, E., "Large elasto-plastic finite element analysis of solids and shells with the enhanced assumed strain concept", *International Journal of Solids and Structures*, vol. 33, no. 20-22, pp. 3215-3237, 1996.

[21] Liu, W. K., Guo, Y., Tang, S., & Belytschko, T., "A multiple-quadrature eight-node hexahedral finite element for large deformation elastoplastic analysis", *Computer Methods in Applied Mechanics and Engineering*, vol. 154, no. 1-2, pp. 69-132, 1998.

[22] Cao, Y. P., Hu, N., Fukunaga, H., Lu, J., & Yao, Z. H., "A highly accurate brick element based on a three-field variational principle for elasto-plastic analysis", *Finite elements in analysis and design*, vol. 39, no. 12, pp. 1155-1171, 2003.

[23] Artioli, E., Castellazzi, G., & Krysl, P., "Assumed strain nodally integrated hexahedral finite element formulation for elastoplastic applications", *International Journal for Numerical Methods in Engineering*, vol. 99, no. 11, pp. 844-866, 2014.

[24] Krysl, P., & Zhu, B., "Locking-free continuum displacement finite elements with nodal integration", *International Journal for Numerical Methods in Engineering*, vol. 76, no. 7, pp. 1020-1043, 2008.

[25] Ayad, R., "Contribution to the numerical modeling of solids and structures and the non-Newtonian fluids forming process: Application to packaging materials", Habilitation to conduct researches, University of Reims, 2002.

[26] Ayad, R., Zouari, W., Meftah, K., Zineb, T. B., & Benjeddou, A., "Enrichment of linear hexahedral finite elements using rotations of a virtual space fiber", *International Journal for Numerical Methods in Engineering*, vol. 95, no. 1, pp. 46-70, 2013.

[27] Meftah, K., Ayad, R., & Hecini, M., "A new 3D 6-node solid finite element based upon the Space Fibre Rotation concept", *European Journal of Computational Mechanics/Revue Européenne de Mécanique Numérique*, vol. 22, no. 1, pp. 1-29, 2013.

[28] Meftah, K., Sedira, L., Zouari, W., Ayad, R., & Hecini, M., "A multilayered 3D hexahedral finite element with rotational DOFs", *European Journal of Computational Mechanics*, vol. 24, no. 3, pp. 107-128, 2015.

[29] Meftah, K., Zouari, W., Sedira, L., and Ayad, R., "Geometric non-linear hexahedral elements with rotational DOFs", *Computational Mechanics*, vol. 57, no. 1, pp. 37-53, 2016.

[30] Simo, J. C., and Taylor, R. L., "Consistent tangent operators for rate-independent elastoplasticity", *Computer methods in applied mechanics and engineering*, vol. 48, no. 1, pp. 101-118, 1985.

[31] Simo, J. C., and Taylor, R. L., "A return mapping algorithm for plane stress elastoplasticity", *International Journal for Numerical Methods in Engineering*, vol. 22, no. 3, pp. 649-670, 1986.

[32] Nayak, G. C., & Zienkiewicz, O. C., "Elasto-plastic stress analysis. A generalization for various constitutive relations including strain softening", *International Journal for Numerical Methods in Engineering*, vol. 5, no. 1, pp. 113-135, 1972.

[33] Peng, Q., and Chen, M. X., "An efficient return mapping algorithm for general isotropic elastoplasticity in principal space", *Computers & Structures*, vol. 92, pp. 173-184, 2012.

[34] Owen, D. R. J., and Hinton, E., "Finite elements in plasticity", Pineridge press, 1980.